

Journal Pre-proof

Evidence for Pleistocene gene flow through the ice-free corridor from extinct horses and camels from Natural Trap Cave, Wyoming

Kieren J. Mitchell, Pere Bover, Alexander T. Salis, Caitlin Mudge, Holly Heiniger, Mary Thompson, Bryan Hockett, Laura S. Weyrich, Alan Cooper, Julie A. Meachen



PII: S1040-6182(21)00558-9

DOI: <https://doi.org/10.1016/j.quaint.2021.11.017>

Reference: JQI 9037

To appear in: *Quaternary International*

Received Date: 30 August 2021

Revised Date: 14 November 2021

Accepted Date: 23 November 2021

Please cite this article as: Mitchell, K.J., Bover, P., Salis, A.T., Mudge, C., Heiniger, H., Thompson, M., Hockett, B., Weyrich, L.S., Cooper, A., Meachen, J.A., Evidence for Pleistocene gene flow through the ice-free corridor from extinct horses and camels from Natural Trap Cave, Wyoming, *Quaternary International* (2021), doi: <https://doi.org/10.1016/j.quaint.2021.11.017>.

This is a PDF file of an article that has undergone enhancements after acceptance, such as the addition of a cover page and metadata, and formatting for readability, but it is not yet the definitive version of record. This version will undergo additional copyediting, typesetting and review before it is published in its final form, but we are providing this version to give early visibility of the article. Please note that, during the production process, errors may be discovered which could affect the content, and all legal disclaimers that apply to the journal pertain.

© 2021 Published by Elsevier Ltd.

1 **Evidence for Pleistocene gene flow through the ice-free corridor from extinct horses and**
2 **camels from Natural Trap Cave, Wyoming**

3
4
5 Kieren J. Mitchell^{a,b,*}, Pere Bover^c, Alexander T. Salis^{a,d}, Caitlin Mudge^a, Holly Heiniger^a, Mary
6 Thompson^e, Bryan Hockett^f, Laura S. Weyrich^{a,g,h}, Alan Cooper^{i,j}, Julie A. Meachen^k

7
8
9 ^a Australian Centre for Ancient DNA, School of Biological Sciences, University of Adelaide, Adelaide, South Australia,
10 Australia

11
12 ^b Otago Palaeogenetics Laboratory, Department of Zoology, University of Otago, Dunedin, New Zealand

13
14 ^c ARAID Foundation, Instituto Universitario de Investigación en Ciencias Ambientales (IUCA) - Aragosaurus Group,
15 Universidad de Zaragoza, Zaragoza, Spain

16
17 ^d Division of Vertebrate Zoology, American Museum of Natural History, New York, New York, USA

18
19 ^e Idaho Museum of Natural History, Idaho State University, Idaho, USA

20
21 ^f US Department of Interior, Bureau of Land Management, Nevada State Office, Reno, Nevada, USA

22
23 ^g Department of Anthropology, Pennsylvania State University, Pennsylvania, USA

24
25 ^h Huck Institutes of the Life Sciences, Pennsylvania State University, Pennsylvania, USA

26
27 ⁱ South Australian Museum, Adelaide, South Australia, Australia

28
29 ^j BlueSky Genetics, Ashton, South Australia, Australia

30
31 ^k Des Moines University, Department of Anatomy, Des Moines, Iowa, USA

32
33 * Corresponding author.

34
35 E-mail address: kieren.j.mitchell@gmail.com (K.J. Mitchell).

Abstract

37

38 Natural Trap Cave (Bighorn Mountains, Wyoming) preserves an abundance of fossil remains from
39 extinct Late Pleistocene fauna and is situated near a past migration route that likely connected
40 populations in Eastern Beringia and the contiguous US—the ice-free corridor between the
41 Cordilleran and Laurentide icesheets. Some palaeontological evidence supports a correspondingly
42 high affinity between fauna recorded in Natural Trap Cave and Eastern Beringia versus elsewhere
43 in the contiguous US, but this hypothesis has not yet been extensively tested using genetic data. In
44 the present study, we analysed 16 horse specimens and one camel specimen from Natural Trap
45 Cave. Of the horse specimens we analysed, we obtained 10 unique and previously unreported
46 mitochondrial haplotypes belonging to two distinct (extinct) genetic clades—two haplotypes
47 corresponded to a caballine horse (*Equus* sp.) and eight corresponded to the stilt-legged horse
48 (*Haringtonhippus francisci*). With only one exception, it appears these newly sequenced individuals
49 all shared a common ancestor more recently with Eastern Beringian individuals than with others
50 from the contiguous US. In addition, mitochondrial data from a specimen assigned to *Camelops*
51 sp. revealed that it shares a closer affinity with specimens from the Yukon Territory than those
52 from Idaho or Nevada, though all appear to belong to a single species (“yesterday’s camel”;
53 *Camelops* cf. *hesternus*). Together, these results are consistent with a high level of genetic
54 connectivity between horse and camel populations in the Bighorn Mountains and Eastern Beringia
55 during the Pleistocene.

56

Keywords

58

59 Phylogenetics; Quaternary; Ancient DNA; Mitogenome; North America; Megafauna

60

1. Introduction

62

63 Throughout the Pleistocene, glacial cycles caused the periodic expansion and contraction of the
64 Cordilleran and Laurentide continental icesheets in the east and west, respectively, of northern
65 North America. During glacial maxima, these two icesheets expanded to the point that they
66 coalesced, likely limiting the dispersal of terrestrial mammals between ice-free areas in Eastern
67 Beringia (Alaska and north-east Canada) and the southern interior of North America (including the
68 modern day contiguous USA). Outside of glacial maxima, an ice-free corridor of varying extent
69 connected these areas and would presumably have permitted faunal dispersal and gene flow.
70 Indeed, fossil data suggest this was the case; for example, morphologically distinct Beringian
71 wolves may have migrated southwards through the ice-free corridor during the Pleistocene prior to
72 the Last Glacial Maximum (Meachen et al., 2016). However, the extent to which the periodic
73 opening and closing of the ice-free corridor influenced the distribution and population structure of

74 Pleistocene fauna, particularly extinct megafauna, has not been extensively tested using genetic
75 data. Ancient DNA is particularly advantageous for studying this phenomenon, because the
76 ancestry and affinities of ancient individuals—including those from extinct species—can be
77 observed directly rather than inferred. However, application of this approach has been limited by
78 relatively poor DNA preservation in ancient specimens from temperate localities in the contiguous
79 US.

80

81 Pleistocene fossils excavated from Natural Trap Cave provide an excellent opportunity to test for
82 past gene flow between animal populations in Eastern Beringia and the North American southern
83 interior (i.e. the contiguous US). Firstly, Natural Trap Cave is situated in the northern Bighorn
84 Mountains, Wyoming, south of the maximum extent of the Pleistocene ice-sheets and very close to
85 the southern terminus of the ice-free corridor (Figure 1). Secondly, fossil remains belonging to a
86 wide range of animal species have been recovered from three distinct periods of deposition—155
87 to 132 thousand years ago, 53 to 17 thousand years ago, and 11 thousand years ago to the
88 present (Lovelace et al., This issue)—spanning multiple glacial cycles. Finally, previous studies
89 have indicated that ancient DNA can successfully be obtained from fossil remains excavated from
90 Natural Trap Cave (e.g. Barnett et al., 2005; Bover et al., 2018; Heintzman et al., 2016; Heintzman
91 et al., 2017; Orlando et al., 2008; Perri et al., 2021; Salis et al., 2020; Salis et al., 2021; Vershinina
92 et al., 2021). Consequently, if dispersal occurred through the ice-free corridor and resulted in gene
93 flow between populations in Eastern Beringia and the contiguous US, this is likely to be reflected in
94 the ancestry of ancient specimens from Natural Trap Cave. Specifically, we might expect to
95 observe a closer affinity between specimens from Natural Trap Cave and Eastern Beringia, as
96 opposed to those from populations further from the southern terminus of the ice-free corridor. We
97 would also expect shared ancestry between specimens from Natural Trap Cave and Eastern
98 Beringia to date to periods when the ice-free corridor would have been traversable—interglacials
99 (e.g. Marine Isotope Stage 3 [MIS 3]).

100

101 Ancient DNA data from North American bison (*Bison* sp.), including specimens from Natural Trap
102 Cave, indicate that bison dispersal through the ice-free corridor likely occurred bi-directionally
103 across multiple glacial cycles (Heintzman et al., 2016). In contrast, the contiguous US appears to
104 have been colonised by brown bears and lions from Eastern Beringia only once, with no evidence
105 for subsequent gene flow (Salis et al., 2020). However, the evidence is less clear-cut either way for
106 other taxa. For example, genetic data have been obtained from the extinct musk-oxen *Bootherium*
107 *bombifrons*—including specimens from Eastern Beringia, Natural Trap Cave, and as far south as
108 Nebraska—but sampling was too sparse to establish a detailed picture of past dispersal and
109 relatedness through time and space (Bover et al., 2018). Similarly, genetic data from caballine
110 (*Equus*) and stilt-legged (*Haringtonhippus*) horses have been obtained from Natural Trap Cave
111 and other southern localities (e.g. Heintzman et al., 2017; Vershinina et al., 2021; Weinstock et al.,

112 2005), but these data are also relatively sparse—complicating conclusions about species-level
113 diversity—and have not specifically been examined in the context of dispersal facilitated by the ice-
114 free corridor.

115

116 Both lineages of horse represented at Natural Trap Cave became extinct at the end of the
117 Pleistocene—after the Last Glacial Maximum but prior to the beginning of the Holocene
118 (Heintzman et al., 2017; Lorenzen et al., 2011; Vershinina et al., 2021). As a result, they have no
119 direct modern descendants from which past gene flow can be inferred. Only ancient DNA from
120 temporally and geographically distributed fossil specimens can reveal detailed patterns of
121 population structure and gene flow for these taxa. Similarly, a genus of endemic North American
122 camels (“yesterday’s camel”; *Camelops*) became extinct at the end of the Pleistocene (Kooyman et
123 al., 2012; Waters et al., 2015), but it remains unclear exactly how many species this genus
124 comprised (Baskin and Thomas, 2016). Genetic data from three *Camelops* individuals from
125 Eastern Beringia have tentatively been referred to *Camelops hesternus* (Heintzman et al., 2015),
126 but the genetic identity and ancestry of more southern populations currently remains untested.
127 Since all these taxa—*Equus*, *Haringtonhippus*, and *Camelops*—were distributed widely across
128 North American prior to their extinction, including both Eastern Beringia and the contiguous US,
129 they are good models for exploring patterns of past migration through the ice-free corridor.

130

131 In this study, we present new mitochondrial genome sequences obtained from 16 horse specimens
132 and one camel specimen excavated from Late Pleistocene deposits in Natural Trap Cave.
133 Because published genetic data for yesterday’s camels are otherwise only available from three
134 Eastern Beringian individuals, we also sequenced mitochondrial genomes from two additional
135 specimens for comparison: one from Spider Cave in Idaho and one from Mineral Hill Cave in
136 Nevada. One additional mitochondrial genome was also obtained from a horse specimen from
137 American Falls Reservoir, Idaho. We used these data to better characterise the phylogenetic
138 affinities of horses and camels from Natural Trap Cave with respect to both those from Eastern
139 Beringia and from populations in the contiguous US further from the southern terminus of the ice-
140 free corridor.

141

142 **2. Material and Methods**

143

144 *2.1 Samples*

145

146 In this study we analysed DNA from a total of 20 fossil specimens, 17 of which were from Natural
147 Trap Cave. Table S1 lists details for all specimens, including provenance, museum accession
148 numbers, and three newly reported radiocarbon ages. All new and previously published
149 radiocarbon ages were calibrated using OxCal v4.4 (Bronk Ramsey, 2016) based on the IntCal20

150 calibration curve (Reimer et al., 2020). All pre-PCR genetic research undertaken as part of this
151 study was conducted in the purpose-built ancient DNA clean-room facilities at the University of
152 Adelaide's Australian Centre for Ancient DNA (ACAD).

153

154 *2.2 DNA extraction*

155

156 To reduce contamination, each sample was UV irradiated for 15 min and then the surface layer
157 was abraded using a Dremel tool with a carborundum cutting disc. Each sample was subsequently
158 powdered using a Mikrodismembrator (Sartorius) or fragmented using a BioPulversiser (BioSpec),
159 and 20-200 mg was transferred to a 2 mL screw-cap tube. 1 mL of 0.5 M EDTA was added, and
160 the sample was incubated at room temperature on a rotary mixer for 30-45 min. Samples were
161 then centrifuged, and the EDTA was removed from the screw-cap tube and discarded. An
162 additional 970 μ L 0.5 M EDTA and 30 μ L 20 mg/mL Proteinase-K were added, and the sample
163 was incubated on a rotary mixer overnight for ~24 hr at 55 °C. The DNA released by these
164 digestion steps was bound and purified using a modified version of a previously published method
165 (Dabney et al., 2013), involving a binding step with a buffer comprising 12.6 mL PB buffer
166 (QIAGEN), 6.5 μ L Tween-20, and 390 μ L NaOAc 3M with in-solution silicon dioxide, followed by
167 two washes with 80% ethanol. Purified DNA was eluted in 200 μ L of TE buffer (10 mM Tris, 1 mM
168 EDTA) with 0.05% Tween-20. Negative (no template) controls were included in each batch of
169 samples to monitor background and cross-contamination.

170

171 *2.3 Library preparation, enrichment, DNA sequencing*

172

173 Illumina DNA sequencing libraries were made from our extracted DNA and negative controls
174 following the protocol of Meyer and Kircher (2010), but using Rohland et al.'s (2015) partial uracil-
175 DNA-glycosylase (UDG) treatment during the end-polishing step and unique 7-mer 5' and 3'
176 barcoded adapters during the ligation step (Rohland and Reich, 2012). We then performed a real-
177 time PCR assay to determine how many cycles of PCR were required to optimise library quantity
178 and complexity (Gamba et al., 2016). Duplicate real-time PCR assays were performed for each
179 library in a final volume of 10 μ L, each comprising 1 μ L of a 1:5 dilution of library, 1 x Platinum Taq
180 DNA Polymerase High Fidelity buffer (ThermoFisher Scientific), 2 mM MgSO₄ (ThermoFisher
181 Scientific), 0.25 mM of each dNTP (ThermoFisher Scientific), 0.4 μ M of each primer
182 (IS7_short_amp_P5 and IS8_short_amp_P7; Meyer and Kircher, 2010), 0.004 x ROX (Life Tech),
183 0.2 x SYBR (Life Tech), 0.56 M DMSO (Sigma-Aldrich), and 0.2 U of Platinum Taq DNA
184 Polymerase High Fidelity (ThermoFisher Scientific), in laboratory grade water. Real-time PCRs
185 were performed on a LightCycler 96 (Roche) with the following cycling conditions: 94 °C for 6 min;
186 40 cycles of 94 °C for 30 s, 60 °C for 30 s, 68 °C for 40 s; followed by a high-resolution melt.
187 Results from our rtPCR suggested substantially fewer cycles were required to amplify libraries

188 created from our samples (11-17 cycles) compared with those made from our negative controls
189 (21-28 cycles), suggesting low DNA template quantities in our controls and negligible levels of
190 cross-contamination.

191

192 The libraries were then amplified using conventional PCR. In order to maintain library complexity
193 and minimise PCR bias, each library was amplified in eight separate 25 μ L reactions, each
194 comprising 3 μ L of undiluted library, 1 x Platinum Taq DNA Polymerase High Fidelity buffer
195 (ThermoFisher Scientific), 2 mM MgSO₄ (ThermoFisher Scientific), 0.25 mM of each dNTP
196 (ThermoFisher Scientific), 0.4 μ M of each primer (IS7_short_amp_P5 and IS8_short_amp_P7;
197 Meyer and Kircher, 2010), and 0.2 U of Platinum Taq DNA Polymerase High Fidelity
198 (ThermoFisher Scientific), in laboratory grade water. Cycling conditions for the PCR were as
199 follows: 94 °C for 6 min; between 11 and 17 cycles (as determined above using rtPCR) of 94 °C for
200 30 s, 60 °C for 30 s, 68 °C for 40 s; and 68 °C for 10 min. The exception was the library made for
201 UW51516, which was subjected to Recombinase Polymerase Amplification (RPA) for 40 min using
202 a TwistAmp Basic kit (TwistDx Inc.) and following the manufacturer's protocol. Amplified libraries
203 were pooled and purified using 1.8 x volume AxyPrep (Axygen), washed twice with 80% ethanol,
204 and then resuspended in 30 μ L of buffer comprising 10 mM Tris, 0.1 mM EDTA, and 0.05%
205 Tween-20.

206

207 All libraries were enriched for placental mammal mitochondrial DNA using hybridisation enrichment
208 with the commercially synthesised RNA probes described by Mitchell et al. (2016). Hybridisation
209 enrichment was performed according to the manufacturer's protocol (Arbor Biosciences: myBaits
210 v3 chemistry) with several modifications: (1) we extended the incubation step to 44 hr (15 hr at 55
211 °C, 16 hr at 50 °C, 17 hr at 55 °C); (2) we used RNA blockers complementary to our truncated
212 library adapters instead of the Blocker #3 provided by the manufacturer; (3) prior to immobilising
213 the RNA baits, we incubated the Dynabeads MyOne Streptavidin C1 (ThermoFisher Scientific) with
214 100 μ g of yeast tRNA to saturate bead sites that bind nucleic acids in a non-specific manner
215 (Llamas et al., 2016); and (4) we washed the RNA baits—once bound to the streptavidin beads—
216 three times by incubating for 5 min at 55 °C with 0.1 SSC and 0.1% SDS (discarding the
217 supernatant after each wash).

218

219 Following, post-enrichment purification, all libraries were eluted in 125 μ L of PCR master mix (1 x
220 PCR buffer, 2.5 mM MgCl₂, 1 mM dNTPs, 0.5 mM primer, 6.25 U AmpliTaq Gold). The master mix
221 from each library was then split into five reactions and subjected to the following thermocycling
222 regime: 94 °C 6 min; 15 cycles of 94 °C for 30 s, 60 °C for 30 s, 72 °C for 45 s; and a final
223 extension of 72 °C for 10 min. Forward and reverse primers included full-length indexed Illumina
224 sequencing adapters (see Meyer and Kircher, 2010). PCR products from each library were pooled

225 and purified using 1.1 x volume AxyPrep (Axygen), washed twice with 80% ethanol, and then
226 resuspended in 30 µL of water.

227

228 *2.4 High-throughput sequencing and data processing*

229

230 All libraries were pooled and sequenced together on either an Illumina NextSeq or HiSeq in paired-
231 end sequencing mode. Raw sequencing reads were demultiplexed using “sabre”
232 (<http://github.com/najoshi/sabre>) according to their unique 7-mer barcode combinations. Using
233 AdapterRemoval v2.1.2 (Schubert et al., 2016) we trimmed residual adapters and low-quality
234 bases (<Phred20 –minquality 4); merged overlapping paired-end reads (minimum overlap = 11 nt);
235 and discarded merged reads <30 bp (–minlength 30). Read quality was visualised using fastQC
236 v0.10.1 (<https://www.bioinformatics.babraham.ac.uk/projects/fastqc/>) before and after trimming to
237 make sure the trimming was efficient.

238

239 Mitochondrial consensus sequences were obtained by mapping all merged reads for each library
240 against a previously published reference sequence for their respective species—KT168321 for
241 stilt-legged horses, KT168318 for caballine horses, and KR822421 for yesterday’s camels—using
242 BWA v0.7.8 (Li and Durbin, 2009; `aln -t 8 -l 1024 -n 0.04 -o 2`). Reads with a mapping quality
243 Phred score >30 were selected and retained using the SAMtools v1.4 (Li et al., 2009) view
244 command (`-q 30`), and duplicate reads were discarded using ‘FilterUniqueSAMCons.py’ (Kircher,
245 2012). A final 75% majority consensus sequence was then generated for each library and checked
246 by eye in Geneious v9.1.6 (<https://www.geneious.com>), calling nucleotides for sites with a
247 minimum depth-of-coverage of 3x. Summary statistics for each consensus sequences are provided
248 in Table S1.

249

250 *2.5 Phylogenetic analyses*

251

252 We aligned our new mitochondrial genome sequences with previously published data (Table S1)
253 using the MUSCLE v3.8.425 (Edgar, 2004) algorithm as implemented in Geneious. Three separate
254 alignments were created: one for stilt-legged horses (n=39; 16,655 bp), one for caballine horses
255 (n=34; 16,662 bp), and one for yesterday’s camels (n=6; 16,681 bp). Ambiguously aligned columns
256 were removed using Gblocks v0.91b (Castresana, 2000) with default settings, which reduced the
257 length of our caballine horse alignment to 16,317 bp. We inferred maximum likelihood phylogenies
258 based on our stilt-legged and caballine horse alignments using IQ-TREE v1.6.11 (Nguyen et al.,
259 2015), with the best-fitting substitution model (HKY+I) selected using ModelFinder (according to
260 the Bayesian Information Criterion) as implemented in IQ-TREE (Kalyaanamoorthy et al., 2017)
261 and 1000 ultrafast bootstrap replicates to assess topological support (Hoang et al., 2017). We

262 created a median-joining haplotype network (Bandelt et al., 1999) from our yesterday's camel
263 alignment using PopART v1.7 (Leigh and Bryant, 2015).

264

265 We used BEAST v1.8.4 (Drummond and Rambaut, 2007) to co-estimate phylogenies, node ages,
266 and tip ages (for specimens without ages measured using radiocarbon dating) using our stilt-
267 legged and caballine horse alignments. We first evaluated the temporal signal in these two
268 alignments using leave-one-out cross-validation (see Stiller et al., 2014) after pruning our
269 alignment to only the sequences from specimens with finite radiocarbon ages (18 stilt-legged
270 horses and 23 caballine horses; see Table S1). Cross validation involved a series of analyses
271 wherein the age of each sample was sequentially omitted and estimated (applying a uniform prior
272 of 0-150 ka—reflecting a range of plausible deposition ages—instead of specifying the radiocarbon
273 age of the specimen). In each case, we applied the best fitting model estimated previously using
274 IQ-TREE (HKY+I), used a strict molecular clock model, and applied a constant population size
275 coalescent tree prior. A uniform prior of 10^{-11} to 10^{-5} substitutions per site per year was placed on
276 the clock rate. The Markov chain Monte Carlo (MCMC) was run for 2×10^6 generations sampling
277 trees and parameter values every 2000 generations. Convergence of parameter values and ESSs
278 > 200 were monitored using Tracer v1.7.1 (Rambaut et al., 2018). For all except one caballine
279 horse, the calibrated radiocarbon age fell within the 95% Highest Posterior Density (95% HPD) of
280 the Bayesian estimate (Table S1), suggesting that our data collectively included sufficient temporal
281 information to estimate the age of undated samples. For the one caballine horse sample that failed
282 cross-validation (IMNH 1136/11898), the estimated age (median = 52.5 ka; 95% HPD = 33.3ka –
283 74.7 ka) was substantially older than the calibrated radiocarbon age (median = 17275 cal BP;
284 CAMS_LLNL-175552), possibly due to contamination of the sample with relatively young carbon
285 (e.g. from adhesives or consolidants; Crann and Grant, 2019) that was not removed prior to
286 radiocarbon dating; as a result, we used the median estimated age from BEAST for this one
287 specimen in all downstream analyses.

288

289 We subsequently performed another series of BEAST analyses wherein those sequences from
290 horse specimens without radiocarbon ages or with infinite radiocarbon ages were sequentially and
291 individually added into their respective alignments in order to estimate the age of the specimens
292 (applying a uniform prior of 0-150 ka on the unknown age). Otherwise, these runs used the same
293 priors and MCMC settings as for the cross-validation analyses described above. Two stilt-legged
294 horse sequences were excluded at this point because their position in the tree precluded accurate
295 date estimate (they were an outgroup to all directly dated samples; Figure 2A). Once all other
296 samples were assigned an age (either based on radiocarbon dating or Bayesian date estimation),
297 we conducted a date-randomisation test for each alignment (Ramsden et al., 2008; Stiller et al.,
298 2014). The date randomisation tests involved assigning each sample an age from the set of all
299 sample ages (sampling without replacement), which we did by extracting the sample ages from our

300 BEAST XML files, re-ordering them according to a randomly assigned integer, and then re-
301 assigning the re-ordered ages to the samples as they were ordered in the original BEAST XML file.
302 For both alignments the posterior substitution rate estimate of the original data did not overlap the
303 95% HPDs of the rate estimates from ten such randomised replicates, suggesting that our dataset
304 could be used to reliably estimate evolutionary rate and divergence times (Figure S1). Again, these
305 date randomisation runs used the same priors and MCMC settings as for the cross-validation.

306
307 We then ran two final BEAST analyses for our stilt-legged horse and caballine horse alignments.
308 These analyses were run as above, except we used an Extended Bayesian Skyline coalescent
309 tree prior, posterior medians for the age of sequences without finite radiocarbon ages, and three
310 separate MCMCs. After removing the first 10% of values sampled by each MCMC, we combined
311 the remaining samples using LogCombiner v1.8.4 and created a maximum clade credibility tree
312 using TreeAnnotator v1.8.4. Convergence of parameter values between the three chains and
313 combined effective sample sizes > 200 were assessed using Tracer v1.7.1. We observed that the
314 inclusion of several sequences in each alignment with >20% indeterminate nucleotides (i.e. coded
315 as N) were contributing to topological uncertainty—reducing branch support across the tree—so
316 we excluded these from our final BEAST analyses (see Table S1; Figure 2A, 3A). Consequently,
317 our final alignments for stilt-legged and caballine horses comprised 32 sequences each.

318
319 In addition to analyses of our horse alignments, we also ran a BEAST analysis for our yesterday's
320 camel alignment. However, because that alignment only contained six sequences—including only
321 three specimens with finite radiocarbon ages (Table S1)—we could not perform the cross-
322 validation or date randomisation tests described above for the stilt-legged and caballine horses.
323 Instead, we constrained the age of the three Eastern Beringian camel specimens with infinite
324 radiocarbon ages using uniform distributions from 50 to 150 ka. We also placed a uniform
325 distribution on the substitution rate of 5.0×10^{-9} to 4.0×10^{-8} substitutions per site per year, which
326 spans a range of values typical for large terrestrial mammals, and we used a constant population
327 size coalescent tree prior. Three separate MCMCs were run for 10^6 generations sampling trees
328 and parameter values every 1000 generations. Otherwise, this analysis was performed using the
329 same settings as for our final analyses of the horse alignments and results were summarised in the
330 same way. Importantly, the posterior ages estimated for camels in this study should only be taken
331 as indicative until they are subject to more rigorous analyses with larger sample sizes that allow for
332 internal validation.

333

334 **3. Results and Discussion**

335

336 *3.1 Stilt-legged horses (Haringtonhippus)*

337

338 Of the 16 horse specimens from Natural Trap Cave that we analysed, 13 yielded mitochondrial
339 haplotypes that showed a close affinity for published sequences from the stilt-legged horse,
340 *Haringtonhippus francisci* (Figure 2A). Eight of these new haplotypes were unique, with the
341 remaining five plausibly representing different specimens from the same individual animals. These
342 eight new haplotypes were all distinct from sequences published by Heintzman et al. (2017), which
343 brings the total number of unique *Haringtonhippus* haplotypes—effectively equivalent to the
344 minimum number of individuals—known from Natural Trap Cave to 14.

345

346 The results of our phylogenetic analyses revealed that 11 of our 13 new *Haringtonhippus*
347 sequences fall within the mitochondrial diversity described by Heintzman et al. (2017), though
348 sequences from Natural Trap Cave do not form a monophyletic clade to the exclusion of
349 sequences from Eastern Beringia or Nevada (Figure 2A). The remaining two sequences—
350 comprising a single unique haplotype—may represent a sister-lineage to all other sequences
351 (Figure 2A). In our view, the genetic distance between these two outgroup sequences and the
352 remaining sequences is unlikely to be of taxonomic significance, although that hypothesis could be
353 tested more rigorously in the future with additional data. Currently, these outgroup specimens have
354 not been directly radiocarbon dated and are also excluded from the results of our Bayesian
355 analysis because the long branch separating them from the remaining samples caused problems
356 with date estimation and convergence of the MCMC (see Section 2.5; Table S1).

357

358 All of the stilt-legged horse sequences from Natural Trap Cave included in our final Bayesian
359 analysis shared a common ancestor more recently with a sequence from Eastern Beringia, and
360 *vice versa*, than with any of the three sequences previously reported from Gypsum Cave in
361 Nevada (Bayesian posterior probability, BPP = 1.0; Figure 2B). This pattern is consistent with
362 ongoing gene flow between Eastern Beringian stilt-legged horse populations and those near to
363 Natural Trap Cave during the Pleistocene, though uncertainty associated with our node age
364 estimates makes the precise timeframe unclear. In addition, high levels of missing data prevented
365 us from confidently determining the affinities of six additional specimens from Natural Trap Cave
366 and one specimen from Mineral Hill Cave, Nevada (see Section 2.5, Figure 2A, Table S1).
367 Consequently, while our results may be suggestive, it is difficult to draw firm conclusions about the
368 connectivity of stilt-legged horse populations in Eastern Beringia and near Natural Trap Cave with
369 those further from the southern terminus of the ice-free corridor (e.g. those in Nevada; Figure 1).

370

371 3.2 Caballine horses (*Equus*)

372

373 Three of our horse specimens from Natural Trap cave yielded caballine horse (*Equus*)
374 mitochondrial haplotypes (Figure 3A)—only two of these were unique, suggesting that they may
375 represent only two different individuals. Vershinina et al. (2021) recently reported caballine horse

376 mitochondrial genome sequences from another four specimens from Natural Trap Cave; however,
377 three of their sequences are identical and could plausibly represent multiple specimens from a
378 single individual animal, especially since radiocarbon ages for all three specimens are practically
379 indistinguishable. Our new data therefore bring the total number of unique caballine horse
380 haplotypes known from Natural Trap Cave to four, which all belong to Vershinina et al.'s (2021)
381 "clade B". Consequently, we only included clade B haplotypes in our downstream analyses. Within
382 North America, clade A haplotypes—specifically A1 and A2 haplotypes—have been reported only
383 from Eastern Beringia and appear to derive from eastward migration across the Bering Land
384 Bridge from Eurasia between 50 and 200 ka (Vershinina et al., 2021).

385

386 As with the stilt-legged horses (Section 3.1, Figure 2), we observed no close affinity between
387 caballine horse sequences from Natural Trap Cave and those obtained from specimens elsewhere
388 in the contiguous US (Figure 3)—represented in our analyses by two sequences from Idaho (one
389 of which we sequenced as part of this study). Instead, one of our new Natural Trap Cave
390 sequences formed a clade with one of Vershinina et al.'s (2021) Natural Trap Cave sequences
391 (BPP = 1.0), which in turn shared a more recent common ancestor with a sequence from Eastern
392 Beringia (BPP = 0.94; Figure 3B), while the remaining two of our new Natural Trap Cave
393 sequences were excluded from our final analysis due to high levels of missing data (see Section
394 2.5, Table S1, Figure 3A). In contrast, Vershinina et al.'s (2021) remaining three sequences from
395 Natural Trap Cave represent a relatively distinct lineage, which last shared a common ancestor
396 with other sequences >100 ka; as for similarly distinct stilt-legged horse lineages from Natural Trap
397 Cave (Section 3.1), this distinct caballine horse lineage may indicate persistent local
398 phylogeographic structure in addition to gene flow with populations in Eastern Beringia.

399

400 Unlike the stilt-legged horse samples from Nevada, which were all closely related (Figure 2), the
401 caballine horse sequences from Idaho were the respective sister lineages to two distinct clades
402 otherwise comprising samples from Eastern Beringia and Natural Trap Cave or Alberta (BPP =
403 0.94 & 1.0, respectively; Figure 3B). The majority of node age estimates within these clades—
404 including the common ancestors of our new Natural Trap Cave sequence and its nearest Eastern
405 Beringian relative—fall within Marine Isotope Stage 3 (MIS 3; 29-57 ka; Figure 3B), when an ice-
406 free corridor was likely present. This is consistent with the occurrence of gene flow between horse
407 populations in Eastern Beringia and those near to Natural Trap Cave via the ice-free corridor prior
408 to coalescence of the ice-sheets during the Last Glacial Maximum. However, age estimates for the
409 common ancestors between these clades and their respective nearest relatives from Idaho (95%
410 HPDs = 65.1-84.9 ka & 50.5-65.9 ka, respectively) substantially overlap with MIS 4 (57-71 ka),
411 when the ice-free corridor may have been inaccessible or less traversable. Together, these
412 observations suggest that populations in the contiguous US, particularly those near to Natural Trap
413 Cave, may have been the source of *Equus* clade B diversity observed in Eastern Beringia during

414 MIS 3, with the majority of gene flow occurring from south to north. This hypothesis is further
415 supported by the apparent absence of *Equus* clade A1 and A2 haplotypes from the contiguous
416 US—otherwise found only in Eastern Beringia—despite increasing the number of samples that
417 were examined by Vershinina et al. (2021).

418

419 3.3 Yesterday's camel (*Camelops*)

420

421 Our Bayesian phylogenetic analysis of yesterday's camel (*Camelops* sp.) included sequences from
422 six specimens: three from Eastern Beringia published by Heintzman et al. (2015), one from Natural
423 Trap Cave, one from Spider Cave in Idaho, and one from Mineral Hill Cave in Nevada (Figure 4A).
424 Our results strongly supported reciprocal monophyly of a clade comprising the sequences from
425 Idaho and Nevada (BPP = 1.0) and a clade comprising the Eastern Beringian sequences and the
426 sequence from Natural Trap Cave (BPP = 1.0). The common ancestor of these two clades
427 occurred between 213 and 836 ka (95% HPD; median = 405 ka; Figure 4B), suggesting that they
428 all likely belong to a single species (*Camelops* cf. *hesternus*; Heintzman et al., 2015). However,
429 our node age estimates for *Camelops* are relatively imprecise and should be treated with caution
430 because they were not estimated using as informative or objective priors compared to our
431 analyses of caballine and stilt-legged horses (see Section 2.5).

432

433 The camel sample from Natural Trap Cave was most closely related to one of the Eastern
434 Beringian samples—YG 328.23—to the exclusion of the remaining two (Figure 4). Our results
435 suggest that the common ancestor of the Natural Trap Cave specimen and its nearest relative
436 occurred between 65.3 and 195 ka (95% HPD; median = 122 ka; Figure 4B). As for the horses
437 (Sections 3.1 & 3.2), this pattern is consistent with greater population connectivity and gene flow
438 between Eastern Beringian populations and those near to Natural Trap Cave versus populations in
439 the contiguous US further from the southern terminus of the ice-free corridor. However, because
440 our dataset includes very few individuals—as for a previous study the extinct musk-oxen
441 *Bootherium bombifrons* (Bover et al., 2018)—this result may be a sampling artefact and needs to
442 be confirmed in the future with more comprehensive sampling.

443

444 3.4 Synthesis

445

446 Contrary to previous work that suggested as many as four distinct horse species were represented
447 among the Pleistocene fossils from Natural Trap Cave (e.g. Eisenmann et al., 2008), genetic data
448 to date—including our new sequences—only provide strong evidence for two species: one species
449 of stilt-legged horse (*Haringtonhippus francisci*) and one species of caballine horse (*Equus* sp.).
450 This conclusion remains true even if the wider mitochondrial diversity described by Vershinina et
451 al. (2021) is interpreted as corresponding to several distinct species (e.g. *Equus ferus*, *E. lambei*,

452 *E. scotti*, *E. occidentalis*), because sequences from Natural Trap Cave all belong to a relatively
453 restricted subset of overall caballine horse diversity (“clade B”; Figure 3). Additional sampling may
454 yet reveal genetic evidence for additional lineages at Natural Trap Cave, but if so they must occur
455 only at very low abundance, having not been detected among the 18 unique horse haplotypes thus
456 far obtained. With respect to abundances, we also note that—assuming horse samples have been
457 randomly chosen for genetic analysis—genetic data are consistent with a roughly three-fold higher
458 abundance of stilt-legged horses versus caballine horses in the Natural Trap Cave assemblage.

459

460 Overall, our results from stilt-legged horses, caballine horses, and yesterday’s camels are all
461 consistent with a higher level of connectivity between populations in Eastern Beringia and those
462 near Natural Trap Cave during the Pleistocene when compared with populations further from the
463 southern terminus of the ice-free corridor (e.g. those in Idaho or Nevada; Figure 1). However, the
464 strength of this conclusion is limited by sparse sampling from localities in the contiguous US other
465 than Natural Trap Cave and the imprecision of our node age estimates, specifically for stilt-legged
466 horses and yesterday’s camels. Greater sampling intensity in future studies may overcome these
467 limitations. Hall’s Cave in Texas, where short fragments of DNA from both *Camelops* and
468 *Haringtonhippus* have been detected in bulk bone samples (Seersholm et al., 2020), may be a
469 promising site for expanding the geographical breadth of datasets for these species. The inclusion
470 of nuclear DNA—if it can reliably be obtained from specimens from the contiguous US—would also
471 help to reveal evidence for finer-scale gene flow that is not captured in the mitochondrial phylogeny
472 of these taxa. Nevertheless, our data reveal intriguing patterns, specifically the lack of strong
473 evidence for southward versus northward dispersal of caballine horses through the ice-free
474 corridor during MIS3. This contrasts with data from bison, brown bears, and lions, which suggest
475 dispersal of these taxa through the ice-free corridor occurred primarily from Eastern Beringia into
476 the contiguous US (Heintzman et al., 2016; Salis et al., 2020), emphasising that patterns of
477 megafaunal dispersal during the Pleistocene are species specific. It may therefore be illuminating
478 to expand sampling of ancient DNA from the contiguous US—including Natural Trap Cave—to
479 include taxa like grey wolves and bighorn sheep, which may also have traversed the ice-free
480 corridor (e.g. Meachen et al., 2016).

481

482 **Author contributions**

483

484 Conceptualisation: KJM, AC, JAM; Investigation: KJM, CM, PB, ATS, HH; Formal analysis: KJM;
485 Data Curation: KJM, CM, PB, ATS, HH, JAM, MT, BH; Resources: KJM, AC, LSW, JAM, MT, BH;
486 Visualisation and Writing (Original Draft): KJM; Writing (Review & Editing): all authors; Funding
487 acquisition: AC, JAM.

488

489 **Data availability**

490

491 Mitochondrial consensus sequences produced as part of this study are available on GenBank
492 (TBA-TBA). Consensus sequences, demultiplexed sequencing reads, and phylogenetic analysis
493 files—including BEAST XMLs—are available through figshare (DOI: TBA).

494

495 **Declaration of competing interests**

496

497 The authors declare that they have no known competing financial interests or personal
498 relationships that could have appeared to influence the work reported in this paper.

499

500 **Acknowledgements**

501

502 We thank the following individuals and organisations for providing permission to analyse samples:
503 Idaho Museum of Natural History, Bureau of Land Management (Brent Breithaupt and Gretchen
504 Hurley), University of Kansas Vertebrate Paleontology, and the University of Wyoming. Samples
505 held by the University of Wyoming were collected from Natural Trap Cave under permit PA13-WY-
506 207 awarded to JAM.

507

508 **Funding**

509

510 Funding for this research was awarded to JAM and AC by the US National Science Foundation
511 (grant EAR/SGP# 1425059) and to AC by the Australian Research Council (grant FL140100260).

512

513 **References**

514

- 515 Bandelt HJ, Forster P, Röhl A. 1999. Median-joining networks for inferring intraspecific
516 phylogenies. *Mol Biol Evol* 16(1):37-48.
- 517 Barnett R, Barnes I, Phillips MJ, Martin LD, Harington CR, Leonard JA, Cooper A. 2005. Evolution
518 of the extinct sabretooths and the American cheetah-like cat. *Curr Biol* 15(15):R589-R590.
- 519 Baskin J, Thomas R. 2016. A review of *Camelops* (Mammalia, Artiodactyla, Camelidae), a giant
520 llama from the Middle and Late Pleistocene (Irvingtonian and Rancholabrean) of North
521 America. *Hist Biol* 28(1-2):120-127.
- 522 Bover P, Llamas B, Thomson VA, Pons J, Cooper A, Mitchell KJ. 2018. Molecular resolution to a
523 morphological controversy: The case of North American fossil muskoxen *Bootherium* and
524 *Symbos*. *Mol Phylogenet Evol* 129:70-76.
- 525 Bronk Ramsey C. 2016. Bayesian analysis of radiocarbon dates. *Radiocarbon* 51(1):337-360.
- 526 Castresana J. 2000. Selection of conserved blocks from multiple alignments for their use in
527 phylogenetic analysis. *Mol Biol Evol* 17(4):540-552.

- 528 Crann CA, Grant T. 2019. Radiocarbon age of consolidants and adhesives used in archaeological
529 conservation. *Journal of Archaeological Science: Reports* 24:1059-1063.
- 530 Dabney J, Knapp M, Glocke I, Gansauge M-T, Weihmann A, Nickel B, Valdiosera C, García N,
531 Pääbo S, Arsuaga J-L, Meyer M. 2013. Complete mitochondrial genome sequence of a
532 Middle Pleistocene cave bear reconstructed from ultrashort DNA fragments. *Proceedings of*
533 *the National Academy of Sciences* 110(39):15758-15763.
- 534 Drummond AJ, Rambaut A. 2007. BEAST: Bayesian evolutionary analysis by sampling trees. *BMC*
535 *Evol Biol* 7(214).
- 536 Edgar RC. 2004. MUSCLE: multiple sequence alignment with high accuracy and high throughput.
537 *Nucleic Acids Res* 32(5):1792-1797.
- 538 Eisenmann V, Howe J, Pichardo M. 2008. Old world hemiones and new world slender species
539 (Mammalia, Equidae). *Palaeovertebrata* 36:159-233.
- 540 Gamba C, Hanghøj K, Gaunitz C, Alfarhan AH, Alquraishi SA, Al-Rasheid KAS, Bradley DG,
541 Orlando L. 2016. Comparing the performance of three ancient DNA extraction methods for
542 high-throughput sequencing. *Molecular Ecology Resources* 16(2):459-469.
- 543 Heintzman PD, Froese D, Ives JW, Soares AER, Zazula GD, Letts B, Andrews TD, Driver JC, Hall
544 E, Hare PG, Jass CN, MacKay G, Southon JR, Stiller M, Woywitka R, Suchard MA,
545 Shapiro B. 2016. Bison phylogeography constrains dispersal and viability of the Ice Free
546 Corridor in western Canada. *Proc Natl Acad Sci U S A* 113(29):8057-8063.
- 547 Heintzman PD, Zazula GD, Cahill JA, Reyes AV, MacPhee RDE, Shapiro B. 2015. Genomic Data
548 from Extinct North American *Camelops* Revise Camel Evolutionary History. *Mol Biol Evol*
549 32(9):2433-2440.
- 550 Heintzman PD, Zazula GD, MacPhee RDE, Scott E, Cahill JA, McHorse BK, Kapp JD, Stiller M,
551 Wooller MJ, Orlando L, Southon J, Froese DG, Shapiro B. 2017. A new genus of horse
552 from Pleistocene North America. *eLife* 6:e29944.
- 553 Hoang DT, Chernomor O, von Haeseler A, Minh BQ, Vinh LS. 2017. UFBoot2: Improving the
554 Ultrafast Bootstrap Approximation. *Mol Biol Evol* 35(2):518-522.
- 555 Kalyaanamoorthy S, Minh BQ, Wong TKF, von Haeseler A, Jermini LS. 2017. ModelFinder: fast
556 model selection for accurate phylogenetic estimates. *Nature methods* 14(6):587-589.
- 557 Kircher M. 2012. Analysis of High-Throughput Ancient DNA Sequencing Data. *Ancient DNA:*
558 *Methods and Protocols*. p 197-228.
- 559 Kooyman B, Hills LV, Tolman S, McNeil P. 2012. Late Pleistocene western camel (*Camelops*
560 *hesternus*) hunting in southwestern Canada. *Am Antiq* 77(1):115-124.
- 561 Leigh JW, Bryant D. 2015. popart: full-feature software for haplotype network construction.
562 *Methods in Ecology and Evolution* 6(9):1110-1116.
- 563 Li H, Durbin R. 2009. Fast and accurate short read alignment with Burrows-Wheeler transform.
564 *Bioinformatics* 25(14):1754-1760.

- 565 Li H, Handsaker B, Wysoker A, Fennell T, Ruan J, Homer N, Marth G, Abecasis G, Durbin R,
566 Subgroup GPD. 2009. The Sequence Alignment/Map (SAM) format and SAMtools.
567 *Bioinformatics* 25(16):2078-2079.
- 568 Llamas B, Fehren-Schmitz L, Valverde G, Soubrier J, Mallick S, Rohland N, Nordenfelt S,
569 Valdiosera C, Richards SM, Rohrlach A, Romero MIB, Espinoza IF, Cagigao ET, Jiménez
570 LW, Makowski K, Reyna ISL, Lory JM, Torrez JAB, Rivera MA, Burger RL, Ceruti MC,
571 Reinhard J, Wells RS, Politis G, Santoro CM, Standen VG, Smith C, Reich D, Ho SYW,
572 Cooper A, Haak W. 2016. Ancient mitochondrial DNA provides high-resolution time scale of
573 the peopling of the Americas. *Science Advances* 2(4).
- 574 Lorenzen ED, Nogues-Bravo D, Orlando L, Weinstock J, Binladen J, Marske KA, Ugan A,
575 Borregaard MK, Gilbert MT, Nielsen R, Ho SY, Goebel T, Graf KE, Byers D, Stenderup JT,
576 Rasmussen M, Campos PF, Leonard JA, Koepfli KP, Froese D, Zazula G, Stafford TW, Jr.,
577 Aaris-Sorensen K, Batra P, Haywood AM, Singarayer JS, Valdes PJ, Boeskorov G, Burns
578 JA, Davydov SP, Haile J, Jenkins DL, Kosintsev P, Kuznetsova T, Lai X, Martin LD,
579 McDonald HG, Mol D, Meldgaard M, Munch K, Stephan E, Sablin M, Sommer RS, Sipko T,
580 Scott E, Suchard MA, Tikhonov A, Willerslev R, Wayne RK, Cooper A, Hofreiter M, Sher A,
581 Shapiro B, Rahbek C, Willerslev E. 2011. Species-specific responses of Late Quaternary
582 megafauna to climate and humans. *Nature* 479(7373):359-364.
- 583 Lovelace DM, Redman CM, Minckley TA, Schubert BW, Mahan S, Wood JR, McGuire JL, Laden J,
584 Bitterman K, Heiniger H, Fenderson L, Cooper A, Mitchell KJ, Meachen JA. This issue. An
585 age-depth model and revised stratigraphy of vertebrate-bearing units in Natural Trap Cave,
586 Wyoming. *Quat Int*.
- 587 Meachen JA, Brannick AL, Fry TJ. 2016. Extinct Beringian wolf morphotype found in the
588 continental U.S. has implications for wolf migration and evolution. *Ecology and Evolution*
589 6(10):3430-3438.
- 590 Meyer M, Kircher M. 2010. Illumina sequencing library preparation for highly multiplexed target
591 capture and sequencing. *Cold Spring Harbor Protocols* 2010(6):1-10.
- 592 Mitchell KJ, Bray SC, Bover P, Soibelzon L, Schubert BW, Prevosti F, Prieto A, Martin F, Austin JJ,
593 Cooper A. 2016. Ancient mitochondrial DNA reveals convergent evolution of giant short-
594 faced bears (Tremarctinae) in North and South America. *Biol Lett* 12(4).
- 595 Nguyen LT, Schmidt HA, von Haeseler A, Minh BQ. 2015. IQ-TREE: a fast and effective stochastic
596 algorithm for estimating maximum-likelihood phylogenies. *Mol Biol Evol* 32(1):268-274.
- 597 Orlando L, Male D, Alberdi MT, Prado JL, Prieto A, Cooper A, Hanni C. 2008. Ancient DNA
598 clarifies the evolutionary history of American late Pleistocene equids. *J Mol Evol* 66(5):533-
599 538.
- 600 Perri AR, Mitchell KJ, Mouton A, Álvarez-Carretero S, Hulme-Beaman A, Haile J, Jamieson A,
601 Meachen J, Lin AT, Schubert BW, Ameen C, Antipina EE, Bover P, Brace S, Carmagnini A,
602 Carøe C, Samaniego Castruita JA, Chatters JC, Dobney K, dos Reis M, Evin A, Gaubert P,

- 603 Gopalakrishnan S, Gower G, Heiniger H, Helgen KM, Kapp J, Kosintsev PA, Linderholm A,
604 Ozga AT, Presslee S, Salis AT, Saremi NF, Shew C, Skerry K, Taranenko DE, Thompson
605 M, Sablin MV, Kuzmin YV, Collins MJ, Sinding M-HS, Gilbert MTP, Stone AC, Shapiro B,
606 Van Valkenburgh B, Wayne RK, Larson G, Cooper A, Frantz LAF. 2021. Dire wolves were
607 the last of an ancient New World canid lineage. *Nature* 591(7848):87-91.
- 608 Rambaut A, Drummond AJ, Xie D, Baele G, Suchard MA. 2018. Posterior Summarization in
609 Bayesian Phylogenetics Using Tracer 1.7. *Syst Biol* 67(5):901-904.
- 610 Ramsden C, Melo FL, Figueiredo LM, Holmes EC, Zanotto PMA, the VC. 2008. High Rates of
611 Molecular Evolution in Hantaviruses. *Mol Biol Evol* 25(7):1488-1492.
- 612 Reimer PJ, Austin WEN, Bard E, Bayliss A, Blackwell PG, Bronk Ramsey C, Butzin M, Cheng H,
613 Edwards RL, Friedrich M, Grootes PM, Guilderson TP, Hajdas I, Heaton TJ, Hogg AG,
614 Hughen KA, Kromer B, Manning SW, Muscheler R, Palmer JG, Pearson C, van der Plicht
615 J, Reimer RW, Richards DA, Scott EM, Southon JR, Turney CSM, Wacker L, Adolphi F,
616 Büntgen U, Capano M, Fahrni SM, Fogtmann-Schulz A, Friedrich R, Köhler P, Kudsk S,
617 Miyake F, Olsen J, Reinig F, Sakamoto M, Sookdeo A, Talamo S. 2020. The IntCal20
618 Northern Hemisphere radiocarbon age calibration curve (0–55 cal kBP). *Radiocarbon*
619 62(4):725-757.
- 620 Rohland N, Harney E, Mallick S, Nordenfelt S, Reich D. 2015. Partial uracil-DNA-glycosylase
621 treatment for screening of ancient DNA. *Philos Trans R Soc Lond B Biol Sci*
622 370(1660):20130624.
- 623 Rohland N, Reich D. 2012. Cost-effective, high-throughput DNA sequencing libraries for
624 multiplexed target capture. *Genome Res* 22(5):939-946.
- 625 Salis AT, Bray SCE, Lee MSY, Heiniger H, Barnett R, Burns JA, Doronichev V, Fedje D,
626 Golovanova L, Harington CR, Hockett B, Kosintsev P, Lai X, Mackie Q, Vasiliev S,
627 Weinstock J, Yamaguchi N, Meachen J, Cooper A, Mitchell KJ. 2020. Lions and brown
628 bears colonized North America in multiple synchronous waves of dispersal across the
629 Bering Land Bridge. *Mol Ecol*. Accepted Author Manuscript.
630 <https://doi.org/10.1111/mec.16267>
- 631 Salis AT, Gower G, Schubert BW, Soibelzon LH, Heiniger H, Prieto A, Prevosti FJ, Meachen J,
632 Cooper A, Mitchell KJ. 2021. Ancient genomes reveal hybridisation between extinct short-
633 faced bears and the extant spectacled bear (*Tremarctos ornatus*).
634 bioRxiv:2021.2002.2005.429853.
- 635 Schubert M, Lindgreen S, Orlando L. 2016. AdapterRemoval v2: rapid adapter trimming,
636 identification, and read merging. *BMC Research Notes* 9:88.
- 637 Seersholm FV, Werndly DJ, Greal A, Johnson T, Keenan Early EM, Lundelius EL, Winsborough
638 B, Farr GE, Toomey R, Hansen AJ, Shapiro B, Waters MR, McDonald G, Linderholm A,
639 Stafford TW, Bunce M. 2020. Rapid range shifts and megafaunal extinctions associated
640 with late Pleistocene climate change. *Nature Communications* 11(1):2770.

- 641 Stiller M, Molak M, Prost S, Rabeder G, Baryshnikov G, Rosendahl W, Münzel S, Bocherens H,
 642 Grandal-d'Anglade A, Hilpert B, Germonpré M, Stasyk O, Pinhasi R, Tintori A, Rohland N,
 643 Mohandesan E, Ho SYW, Hofreiter M, Knapp M. 2014. Mitochondrial DNA diversity and
 644 evolution of the Pleistocene cave bear complex. *Quat Int* 339-340:224-231.
- 645 Vershinina AO, Heintzman PD, Froese DG, Zazula G, Cassatt-Johnstone M, Dalén L, Der
 646 Sarkissian C, Dunn SG, Ermini L, Gamba C, Groves P, Kapp JD, Mann DH, Seguin-
 647 Orlando A, Southon J, Stiller M, Wooller MJ, Baryshnikov G, Gimranov D, Scott E, Hall E,
 648 Hewitson S, Kirillova I, Kosintsev P, Shidlovsky F, Tong H-W, Tiunov MP, Vartanyan S,
 649 Orlando L, Corbett-Detig R, MacPhee RD, Shapiro B. 2021. Ancient horse genomes reveal
 650 the timing and extent of dispersals across the Bering Land Bridge. *Mol Ecol*.
- 651 Waters MR, Stafford TW, Kooyman B, Hills LV. 2015. Late Pleistocene horse and camel hunting at
 652 the southern margin of the ice-free corridor: Reassessing the age of Wally's Beach,
 653 Canada. *Proc Natl Acad Sci U S A* 112(14):4263.
- 654 Weinstock J, Willerslev E, Sher A, Tong W, Ho SYW, Rubenstein D, Storer J, Burns J, Martin L,
 655 Bravi C, Prieto A, Froese D, Scott E, Xulong L, Cooper A. 2005. Evolution, Systematics,
 656 and Phylogeography of Pleistocene Horses in the New World: A Molecular Perspective.
 657 *PLoS Biol* 3(8):e241.

658

659 **Figure captions**

660

661 **Figure 1 (colour):** Map of study areas relative to the location of the Cordilleran and Laurentide ice
 662 sheets and the ice-free corridor connecting Eastern Beringia (dark gray) to locations in the
 663 contiguous US (adapted from Meachen et al., 2016). Depiction approximates extent during
 664 Pleistocene glacial minima; during glacial maxima the ice sheets would likely have coalesced and
 665 no ice-free corridor would have been present. Natural Trap Cave (blue circle) in Wyoming (blue) is
 666 closer to the southern terminus of the ice-free corridor compared to study sites in Idaho (orange;
 667 light and dark orange circles) or Nevada (red; light and dark red circles).

668

669 **Figure 2 (colour):** A) Maximum likelihood phylogeny of stilt-legged horse (*Haringtonhippus*
 670 *francisci*) mitochondrial genome sequences. Ultrafast bootstrap support from IQ-TREE is displayed
 671 for nodes with 95% support or higher. Tips are labelled with a shorthand reference number (see
 672 Table S1) and specimen ID; new sequences obtained as part of this study are marked with an
 673 asterisk. Coloured circles indicate geographical provenance of samples. Branch lengths are
 674 proportional to number of substitutions; scale is in number of substitutions per site. Sequences
 675 labelled in light grey were excluded from our final Bayesian analysis due to either a high number of
 676 indeterminate nucleotides (given in brackets following the specimen ID) or inability to confidently
 677 estimate the age of the specimens (see Section 2.5 and Table S1). B) Time-calibrated Bayesian
 678 phylogeny of stilt-legged horse mitochondrial genome sequences. Coloured circles indicate

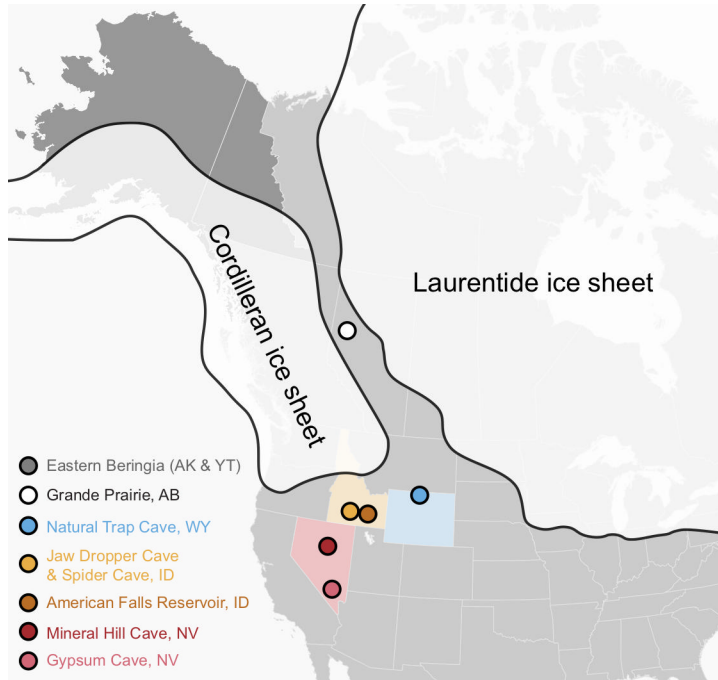
679 geographical distribution of samples. Samples are labelled with a shorthand reference (see Table
680 S1) and new sequences are marked with an asterisk. Shaded vertical bars demarcate Marine
681 Isotope Stages 1 through 7 (even numbered MISs are colder glacials while odd numbered MISs
682 are warmer interglacials). Branch lengths are proportional to time (scaled in thousands of years
683 before present). Tip and node heights are plotted as median values. Horizontal node bars reflect
684 95% Highest Posterior Densities (95% HPDs). Labels reflect Bayesian posterior probability (only
685 displayed for branches with a value of at least 0.90).

686

687 **Figure 3 (colour):** A) Maximum likelihood phylogeny of caballine horse mitochondrial genome
688 sequences corresponding to Vershinina et al.'s (2021) *Equus* sp. "clade B". Ultrafast bootstrap
689 support from IQ-TREE is displayed for nodes with 95% support or higher. Tips are labelled with a
690 shorthand reference number (see Table S1) and specimen ID; new sequences obtained as part of
691 this study are marked with an asterisk. Coloured circles indicate geographical provenance of
692 samples. Branch lengths are proportional to number of substitutions; scale is in number of
693 substitutions per site. Sequences labelled in light grey were excluded from our final Bayesian
694 analysis because they comprised a high number of indeterminate nucleotides (given in brackets
695 following the specimen ID; see Section 2.5 and Table S1). B) Time-calibrated Bayesian phylogeny
696 of caballine horse mitochondrial genome sequences. Coloured circles indicate geographical
697 distribution of samples. New sequences are marked with an asterisk. Shaded bars demarcate
698 Marine Isotope Stages 1 through 6 (even numbered MISs are colder glacials while odd numbered
699 MISs are warmer interglacials). Branch lengths are proportional to time (scaled in thousands of
700 years before present). Tip and node heights are plotted as median values. Node bars reflect 95%
701 Highest Posterior Densities (95% HPDs). Labels reflect Bayesian posterior probability (only
702 displayed for branches with a value of at least 0.90).

703

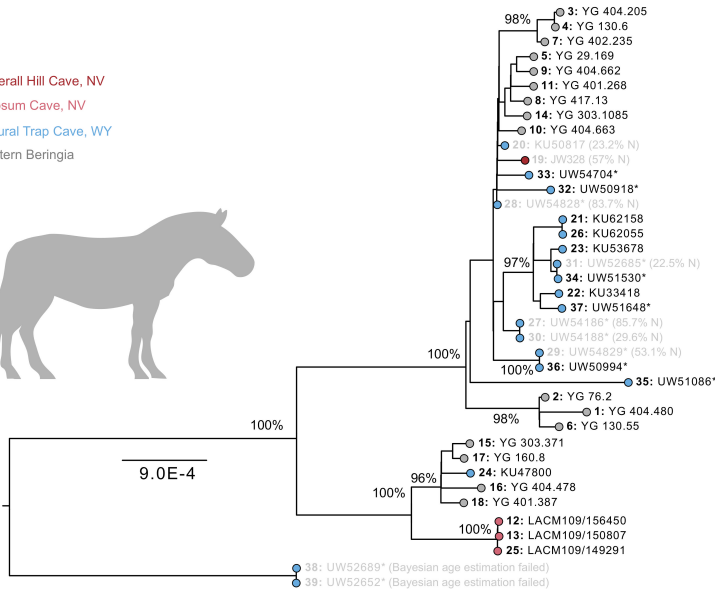
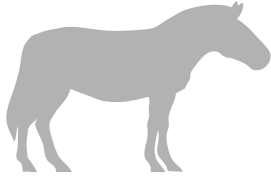
704 **Figure 4 (colour):** A) Median-joining haplotype network for yesterday's camel (*Camelops* sp.)
705 mitochondrial genome sequences from Natural Trap Cave (blue circle), Spider Cave (orange
706 circle), Mineral Hill Cave (red circle), and Eastern Beringia (grey circle). Tips are labelled in with a
707 shorthand reference number (see Table S1) and new sequences are marked with an asterisk.
708 Network edges are labelled with the number of substitutions separating haplotypes. B) Time-
709 calibrated Bayesian phylogeny of yesterday's camel mitochondrial genome sequences. Branch
710 lengths are proportional to time (in thousands of years before present); tip and node heights are
711 median values; node bars reflect 95% Highest Posterior Densities (95% HPDs). Labels reflect
712 Bayesian posterior probability.



Journal Pre-proof

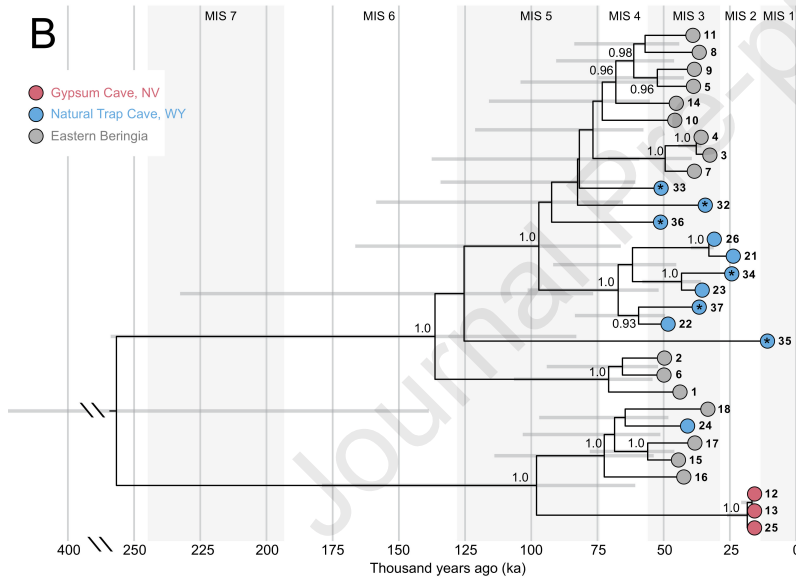
A

- Mineraill Hill Cave, NV
- Gypsum Cave, NV
- Natural Trap Cave, WY
- Eastern Beringia

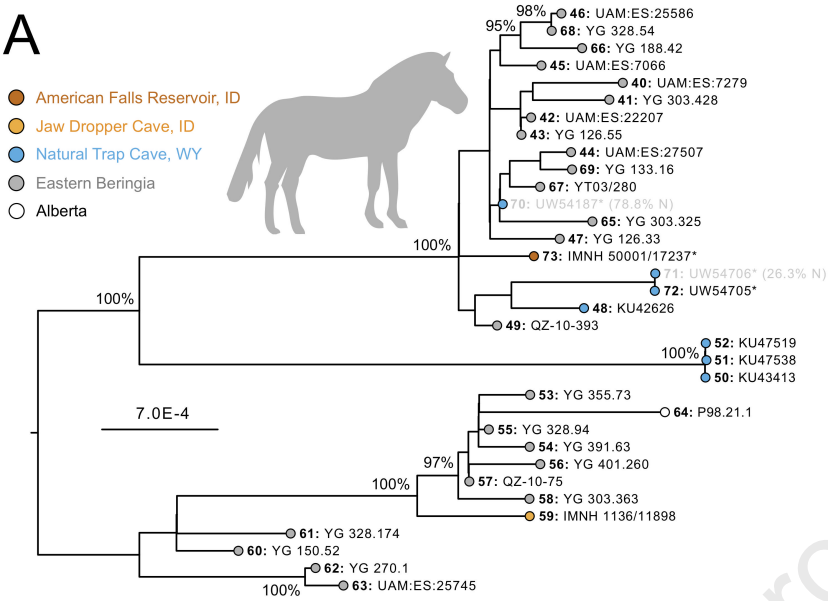


B

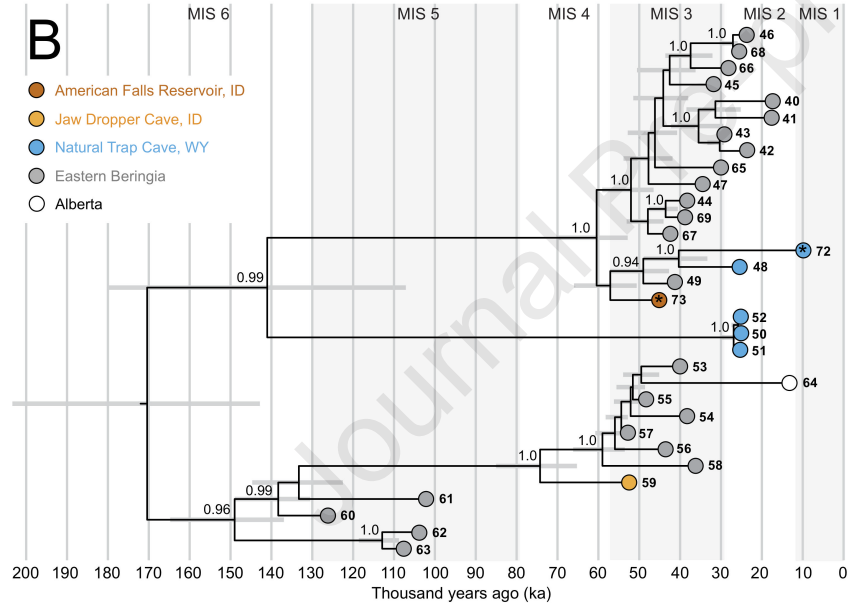
- Gypsum Cave, NV
- Natural Trap Cave, WY
- Eastern Beringia

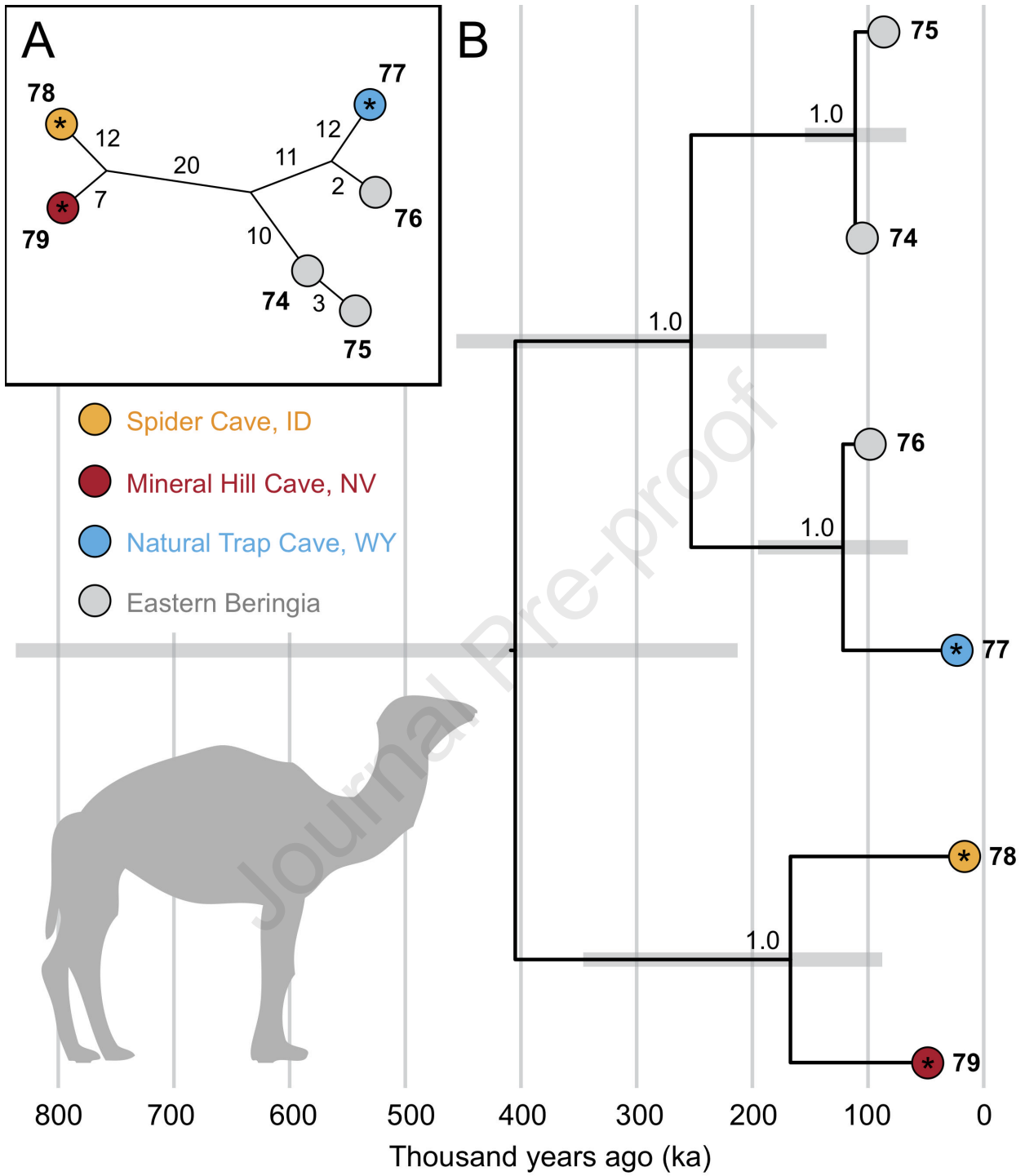


A



B





Declaration of interests

The authors declare that they have no known competing financial interests or personal relationships that could have appeared to influence the work reported in this paper.

~~The authors declare the following financial interests/personal relationships which may be considered as potential competing interests:~~

Journal Pre-proof